Received: 8 December 2025 | Revised: 23 February 2026 | Accepted: 10 March 2026 | Published online: 26 March 2026

RESEARCH ARTICLE

Medinformatics
2026, Vol. 00(00) 1–15
DOI: 10.47852/bonviewMEDIN62028733

BON VIEW PUBLISHING

Beyond Sunscreen Multitarget Docking of Mycosporine-Like Amino Acids (MAAs) for Anti-aging, Neuroprotection, and Immunomodulation

Varsha K. Singh[1], Niharika Sahu[1] and Rajeshwar P. Sinha[1,*]

[1] *Department of Botany, Banaras Hindu University, India*

Abstract: Mycosporine-like amino acids (MAAs) act as efficient photoprotective and antioxidant agents, safeguarding biological systems from ultraviolet-induced oxidative damage. Owing to their biocompatibility and stability, MAAs have gained significant attention as eco-friendly bioactives in cosmetic and dermatological formulations. While previous research has primarily focused on their photoprotective roles, limited attention has been given to their broader therapeutic potential. Emerging evidence suggests that these compounds may influence multiple biochemical pathways related to aging, neural health, and immune function. However, systematic investigations into their molecular interactions with diverse biological targets are still limited. In the present study, we address this knowledge gap through a comprehensive multitarget molecular docking analysis of 32 structurally diverse MAAs against four key human proteins implicated in oxidative stress, neurodegeneration, and immune modulation. The selected targets include acetylcholinesterase (4EY7) for neuroprotection, matrix metalloproteinase-1 (3SHI) for anti-aging, Keap1 (1U6D) for oxidative stress regulation, and cyclooxygenase-2 (5IKR) for immunomodulation. This integrative computational approach aims to elucidate the multitarget therapeutic potential of MAAs, highlighting their prospective roles beyond conventional UV photoprotection. Our findings demonstrate promising binding interactions between several MAAs and these target proteins, suggesting potential inhibitory and regulatory effects across multiple physiological systems. These results highlight the multitarget binding potential of MAAs and suggest possible pharmacological relevance that warrants further experimental validation. The study thus redefines the scope of MAAs, presenting them not merely as photoprotective compounds but as versatile biomolecules with wide-ranging pharmacological relevance.

Keywords: anti-aging, immunomodulatory, MAAs, neuroprotection, oxidative stress

1. Introduction

Mycosporine-like amino acids (MAAs) represent a structurally diverse group of small, highly water-soluble secondary metabolites synthesized by a wide array of organisms ranging from cyanobacteria and micro- and macro-algae to fungi, lichens, and certain marine invertebrates that are exposed to intense solar UV radiation [1]. Typically, MAAs are built around either an aminocyclohexenone or aminocyclohexenimine core, which is often modified by the addition of amino acid or amino alcohol substituents, thereby influencing spectral and chemical properties [2]. These compounds are distinguished by their ability to absorb UV-A and UV-B radiation, combined with remarkable photostability and efficient conversion of excitation energy into harmless heat, rendering them nature's own molecular sunscreens [1]. Their absorption maxima (λmax) typically span the wavelength region from approximately 309 nm to 362 nm, depending on molecular substitution and ring structure, and many MAAs exhibit high molar extinction coefficients (ε), underscoring their effectiveness in UV screening.

Beyond their UV-screening capacity, accumulating evidence highlights multifunctional bioactivities of MAAs. They have been shown to act as antioxidants, scavenging reactive oxygen species and thereby mitigating oxidative stress, a key contributor to cellular aging and neurodegeneration [3]. In addition, MAAs display anti-inflammatory, anti-aging, wound healing, and even immunomodulatory properties, suggesting that their biological effects may extend beyond cosmetic photoprotection [4]. Several review articles have summarized aspects of their chemistry, biosynthesis, and photoprotective functions [5–7]. However, these reviews often emphasize specific features (e.g., UV absorption or ecological distribution) and do not always address the broader multitarget molecular interactions that MAAs may have in human health-relevant pathways. Therefore, we hypothesize that MAAs are capable of interacting with multiple human protein targets involved in oxidative stress regulation, extracellular matrix (ECM) degradation, neurotransmission, and inflammatory signaling and that such interactions may contribute to their reported multifunctional biological effects.

***Corresponding author:** Rajeshwar P. Sinha, Department of Botany, Banaras Hindu University, India. Email: rpsinha@bhu.ac.in

To investigate the potential multifunctional roles of MAAs in aging, neurodegeneration, oxidative stress, and immune regulation, four human protein targets with well-established biomedical relevance were selected for molecular docking. Each target was chosen for its critical role in a specific pathological pathway: matrix metalloproteinase (MMP-1) as a key driver of collagen breakdown and skin aging, AChE as a central regulator of cholinergic signaling and cognitive decline, Keap1 as the principal modulator of the nuclear factor erythroid 2–related factor 2 (Nrf 2) antioxidant response, and cyclooxygenase (COX-2) as a major mediator of inflammatory and immune pathways. By targeting these proteins, the study focuses on complementary and clinically relevant axes to evaluate whether MAAs may exert broad multifunctional biological effects beyond their known photoprotective role.

Acetylcholinesterase (AChE; PDB ID: 4EY7) is a critical enzyme in the cholinergic neurotransmission system, catalyzing the hydrolysis of acetylcholine into choline and acetic acid at neuronal synapses. Its excessive inhibition or dysfunction results in cholinergic imbalance, leading to cognitive decline and neurodegenerative disorders such as Alzheimer's disease. The 4EY7 crystal structure, resolved at 2.35 Å with donepezil as the co-crystallized ligand, provides a well-characterized model for assessing neuroprotective activity through AChE modulation [8, 9].

MMP-1) PDB ID: 3SHI), a zinc- and calcium-dependent endopeptidase, catalyzes the degradation of interstitial collagens (types I–III) within the ECM. Overexpression of MMP-1 contributes to photoaging and dermal collagen loss, resulting in wrinkle formation and reduced skin elasticity. The catalytic domain structure (2.20 Å) offers a reliable framework for studying anti-aging or collagen-protective interactions. [10–12].

Kelch-like ECH-associated protein 1 (Keap1; PDB ID: 1U6D) serves as a cytoplasmic oxidative stress sensor, regulating the structural destabilization of Nrf2 through the ubiquitin–proteasome pathway. Under oxidative conditions, Keap1 cysteine residues undergo conformational changes that prevent Nrf2 degradation, leading to the activation of antioxidant and detoxification genes. The β-propeller structure of the 1U6D Kelch domain reveals the ETGE-motif binding pocket crucial for Keap1–Nrf2 interaction, making it a prime target for discovering antioxidant response activators [13, 14].

COX-2 (PDB ID: 5IKR), also known as prostaglandin-endoperoxide synthase-2, is an inducible enzyme responsible for catalyzing the conversion of arachidonic acid into prostaglandin H_2, a precursor of prostaglandins involved in pain, inflammation, and immune responses. Its crystal structure (2.34 Å) in complex with mefenamic acid, a nonsteroidal anti-inflammatory drug, illustrates the substrate-binding channel and inhibitory interactions within the cyclooxygenase domain, supporting its role as a key immunomodulatory target [15, 16].

Collectively, these four targets encompass critical biochemical axes, AChE for neurodegeneration, MMP-1 for skin aging, Keap1 for oxidative defense, and COX-2 for inflammation control. By docking a panel of 32 structurally diverse MAAs against these proteins, this study aims to elucidate their potential as multifunctional bioactives, offering a unified molecular perspective on anti-aging, neuroprotective, and immunomodulatory mechanisms beyond their established photoprotective role. Figure 1 summarizes the workflow of our study.

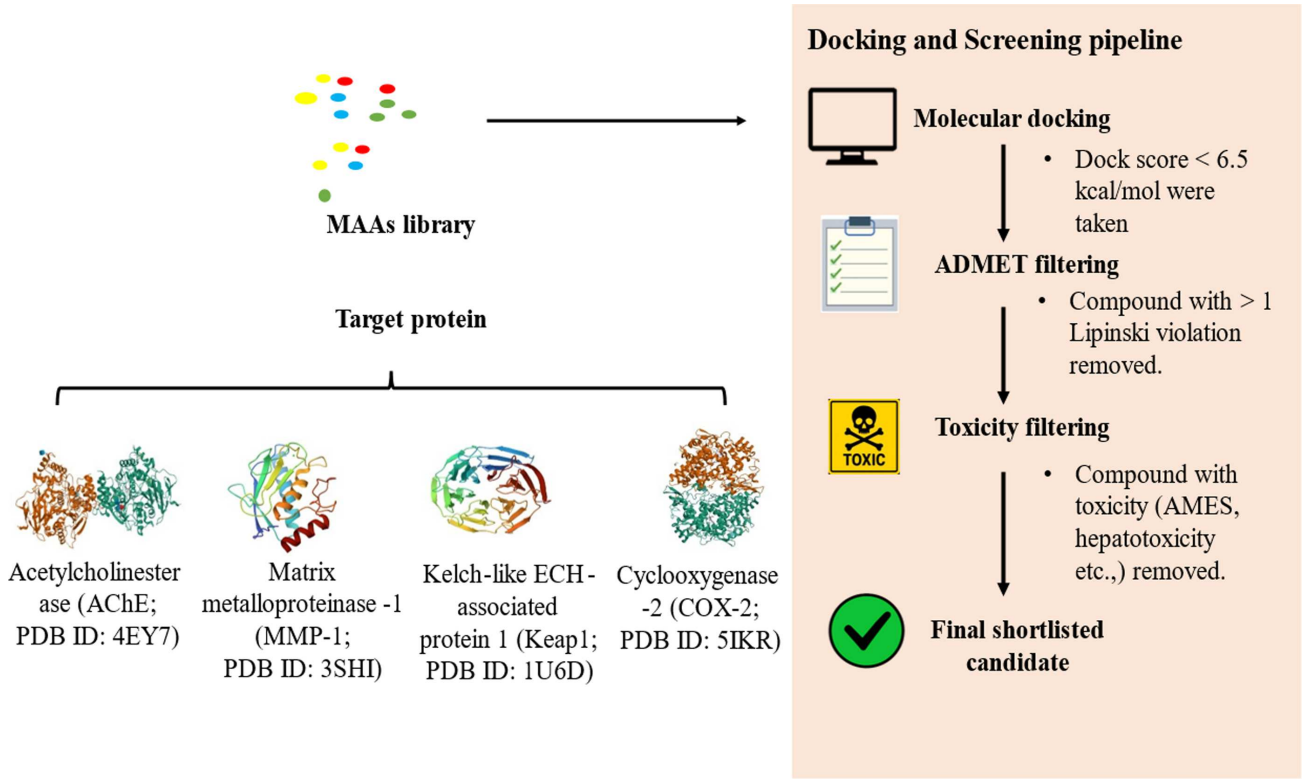

Figure 1. Overview of the virtual screening and molecular docking workflow used for selecting potential bioactive MAAs against key therapeutic target proteins

2. Materials and Methods

2.1. Ligand selection and preparation

A set of 32 MAAs was chosen based on their structural diversity and reported biological relevance from existing literature and compound databases. The two-dimensional (2D) structures of the selected MAAs were sourced in SDF format from the PubChem database and subsequently converted into three-dimensional (3D) conformations using Pymol. All selected MAAs were energy-minimized using the Open Babel minimizer implemented in PyRx (Python Prescription 0.8), while AutoDock-Tools (version 1.5.7, The Scripps Research Institute, La Jolla, CA, USA) was used for adding polar hydrogens, assigning Gasteiger charges, and converting the structures to PDBQT format for docking [17, 18].

2.2. Protein target selection and preparation

Four target proteins representing key biological processes—that is, aging, neurodegeneration, and immune regulation—were selected for docking: 4EY7, human acetylcholinesterase (AChE), central to cholinergic neurotransmission; 3SHI, human collagenase (MMP-1), associated with skin aging and collagen degradation; 1U6D, Keap1, serves as a cytoplasmic oxidative stress sensor; and 5IKR, cyclooxygenase-2, a regulator of immune and inflammatory signaling.

Resolved protein structures were obtained from the Protein Data Bank (PDB) [19]. Each structure was preprocessed using AutoDock Tools (v1.5.7) by removing water molecules, co-crystallized ligands, and heteroatoms. Kollman charges were assigned, polar hydrogens were added, and the proteins were converted into PDBQT format. For proteins that contained co-crystallized (native) ligands, the grid box for docking was centered around the native ligand coordinates to define the active site. For targets that lacked native ligands, the CASTp server (Computed Atlas of Surface Topography of Proteins) (http://sts.bioe.uic.edu) was employed to identify potential binding pockets and determine their geometric centers and pocket volumes [20, 21]. These coordinates were subsequently used to define the docking grid parameters.

2.3. Molecular docking

Docking simulations were performed using AutoDock Vina (v1.5.7) (http://vina.scripps. edu) to predict the most favorable binding conformations and interactions between MAAs and the selected protein targets [12]. Each receptor was rigid, while the ligands were allowed full torsional flexibility. For each receptor, the docking grid was defined based on either the native ligand position or the largest pocket predicted by the CASTp server [22].

2.4. Validation of docking protocol

The docking protocol was validated to ensure the reliability and reproducibility of the results. For proteins with native ligands (4EY7 and 3SHI), re-docking was performed, and the resulting poses showed root mean square deviation (RMSD) values below 2.0 Å, confirming the accuracy of the docking parameters. For the protein without a native ligand (1U6D and 5IKR), consistency of the docking approach was verified by performing multiple independent docking runs using CASTp-defined grid centers, which produced reproducible binding orientations across simulations [23]. To enhance methodological robustness, docking parameters were standardized across all targets, including consistent exhaustiveness values and grid definitions centered on experimentally validated binding pockets or CASTp-predicted cavities. The docking threshold (≤ -6.5 kcal/mol) was selected based on reported literature benchmarks where values below this range typically suggest energetically favorable ligand–receptor interactions. However, we acknowledge that docking scores are relative estimates and should be interpreted comparatively rather than as absolute measures of binding strength.

2.5. Pharmacokinetics analysis

The chosen ligands were analyzed through ADME (Absorption, Distribution, Metabolism, and Excretion) profiling to predict their drug-likeness and pharmacological suitability. Parameters such as molecular weight (MW), hydrogen bond donors (HBD) and acceptors (HBA), topological polar surface area (TPSA), rotatable bonds, lipophilicity (LogP), and water solubility were computed using freely accessible web-based platforms SwissADME (accessed at http://www.swissadme.ch/). Compliance with Lipinski's rule of five, the BOILED-Egg model was assessed to estimate oral bioavailability, human intestinal absorption, and blood–brain barrier (BBB) permeability [24, 25].

2.6. Toxicity assessment

Toxicological assessments were carried out using OSIRIS property explorer software, which serves to predict parameters such as mutagenicity, carcinogenicity, and skin irritation and reproductive effects, along with evaluation of drug score (DS) and drug-likeness of selected hits [14]. The PkCSM tool was used to evaluate the oral toxicity risk of the shortlisted hit ligands. Compounds exhibiting severe toxicity risks or failing multiple ADME criteria were excluded from further consideration [26]. This integrative workflow ensured that only ligands demonstrating strong binding affinity (≤ -6.5 kcal mol^{-1}), acceptable pharmacokinetic characteristics, and favorable toxicity profiles were prioritized for subsequent discussion as potential multifunctional bioactive candidates.

2.7. Visualization and interaction analysis

Docked complexes were analyzed using a combination of 2D and 3D visualization tools to elucidate the interaction patterns and spatial conformations of the MAAs with their respective protein targets. The top ligands, selected based on lowest binding energy as well as favorable ADME and toxicity profiles, were examined in Discovery Studio Visualizer (v2021) to evaluate the overall ligand orientation within the binding pocket, assess the depth and complementarity of the active site, and confirm key interactions such as hydrogen bonding, π–π stacking, and hydrophobic contacts in 3D space [27].

2.8. Computational environment

All computational analyses were performed on a Windows 10 workstation equipped with an Intel Core i7 processor (3.6 GHz), 16 GB RAM, and an NVIDIA GeForce GPU (4 GB VRAM). AutoDock Tools and AutoDock Vina (v1.5.7) were used

for ligand preparation, grid box generation, and docking execution. All visualizations and post-docking analyses were conducted using Discovery Studio Visualizer (v2021).

3. Results and Discussions

3.1. Target protein retrieval and preparation

The protein sequences were procured in FASTA format from the RCSB Protein Data Bank (PDB IDs: 4EY7; 3SHI; 1U6D; 5IKR). The proteins were selected as promising candidates based on an extensive review of the existing literature. The CASTp web-based tool was employed to identify and analyze binding pockets on the target proteins through geometry-driven computational approaches. The binding site in the chains, denoted by the residue, was identified and confirmed by the server CASTpfold. The pocket ID with maximum Area (A2) and Volume (A3) was chosen for determining the residues [11].

3.2. Biomolecules docking study

The grid box parameters (center coordinates and dimensions) used in AutoDock Vina (v1.5.7) for all targets are summarized in Table 1. The docking algorithm generated multiple binding poses per ligand, and the conformation with the lowest binding energy and most favorable interaction profile was selected for further analysis. Following molecular docking, ligands exhibiting a binding affinity equal to or better than −6.5 kcal mol^{-1} were considered to possess significant binding potential and were selected for pharmacokinetic and toxicity evaluations. This threshold was chosen based on literature consensus, where docking scores below −6.5 kcal mol^{-1} generally indicate a plausible and energetically favorable interaction within the target binding pocket. Table 2 includes a comprehensive overview of all the screened compounds, specifying their PubChem compound ID, molecular formula, and docking scores (in Kcal/mol) relative to the target receptor.

Table 1. Details of grid box parameters utilized for docking analysis

Target protein	Center			Size			Energy_range	Exhaustiveness
	x	y	z	x	y	z		
4EY7	10.945464	-56.551464	-23.467893	60	60	60	4	8
3SHI	4.923	-16.094	-10.721	40	46	52	4	8
1U6D	5.164	27.945	64.922	66	72	108	4	8
5IKR	46.045	35.464	91.964	60	60	60	4	8

Table 2. List of selected MAAs with their respective PubChem ID, molecular formula, and docking score with four different target proteins (selected hits for further assessment are mentioned in bold)

Cyanobacterial photoprotective compounds	PubChem compound ID	Molecular formula	Docking score (kcal/mol)			
			4EY7	3SHI	1U6D	5IKR
Aplysiapalythine-A	171119293	$C_{13}H_{23}N_2O_6$	–7.2	–6.2	–6.4	–6.0
Aplysiapalythine-B	171119294	$C_{12}H_{21}N_2O_5$	–7.4	–5.9	–7.1	–5.8
Aplysiapalythine -C	171119295	$C_{11}H_{19}N_2O_5$	–6.4	–5.9	–7.4	–5.9
Asterina-330	13194807	$C_{12}H_{20}N_2O_6$	–7.6	–6.3	–5.9	–6.9
Deoxygadusol	85926716	$C_8H_{12}O_5$	–6.1	–6.0	–6.8	–6.2
Euhalothece-362	139587792	$C_{14}H_{22}N_2O_7$	–7.6	–7.0	–7.0	–7.2
Gadusol	195955	$C_8H_{12}O_6$	–6.5	–6.3	–7.0	–6.5
Mycosporine-methylamine-serine	171990363	$C_{11}H_{18}N_2O_5$	–6.8	–6.0	–7.5	–7.0
Mycosporine-serinol	4485537	$C_{11}H_{19}NO_6$	–6.7	–6.0	–6.3	–6.8
Mycosporine-taurine	155802258	$C_{10}H_{17}NO_7S$	–5.7	–6.4	–7.4	–6.8
Mycosporine-2-glycine	23427657	$C_{12}H_{18}N_2O_7$	–8.0	–6.8	–6.2	–7.4
Mycosporine-GABA	146683910	$C_{12}H_{19}NO_6$	–7.2	–6.6	–7.4	–6.3
Mycosporine-glutamicol	9882880	$C_{13}H_{21}NO_7$	–7.3	–6.9	–7.7	–5.8
Mycosporine-glutamine	101835612	$C_{13}H_{20}N_2O_7$	–8.0	–6.6	–8.4	–6.4
Mycosporine-glutaminol	138756215	$C_{13}H_{22}N_2O_6$	–7.1	–5.9	–8.0	–6.0
Mycosporine-glycine-valine	101016647	$C_{15}H_{24}N_2O_7$	–6.6	–6.7	–7.9	–6.1
Mycosporine-glycine	14444486	$C_{10}H_{15}NO_6$	–7.0	–6.2	–7.6	–7.1
Mycosporine- glutamic acid- glycine	155802374	$C_{15}H_{22}N_2O_9$	–7.1	–6.9	–7.5	–6.5
Mycosporine-hydroxyglutamicol	101805382	$C_{13}H_{21}NO_8$	–7.2	–6.3	–8.2	–7.7
Mycosporine-lysine	146684856	$C_{14}H_{24}N_2O_6$	–6.8	–6.4	–7.0	–7.7

(*Continued*)

Table 2. (*Continued*)

Cyanobacterial photoprotective compounds	PubChem compound ID	Molecular formula	Docking score (kcal/mol)			
			4EY7	3SHI	1U6D	5IKR
Mycosporine-methylamine-threonine	21773596	$C_{13}H_{22}N_2O_6$	–8.1	–6.3	–6.8	–7.4
Mycosporine-ornithine	146684857	$C_{13}H_{22}N_2O_6$	–7.4	–7.0	–6.7	–7.0
Mycosporine-glycine-alanine	102110164	$C_{13}H_{20}N_2O_7$	–7.6	–6.0	–6.5	–6.7
Palythenic acid	101016648	$C_{14}H_{20}N_2O_7$	–8.2	–6.8	–6.9	–6.2
Palythene	21773785	$C_{13}H_{20}N_2O_5$	–7.8	–6.8	–6.5	–6.5
Palythine	16047608	$C_{10}H_{16}N_2O_5$	–7.4	–6.7	–6.1	–7.3
Palythine-serine	1774828	$C_{11}H_{18}N_2O_6$	–7.2	–6.7	–6.1	–7.3
Palythine-threonine	155802074	$C_{12}H_{20}N_2O_6$	–7.5	–6.9	–6.3	–6.0
Palythinol	9948334	$C_{13}H_{22}N_2O_6$	–7.7	–6.3	–7.4	–5.9
Porphyra-334	6857486	$C_{14}H_{22}N_2O_6$	–6.9	–6.7	–7.8	–7.9
Usujirene	15847474	$C_{13}H20N_2O_5$	–6.7	–6.6	–6.2	–6.6
Shinorine	10471931	$C_{13}H_{20}N_2O_8$	–7.6	–6.3	–7.9	–7.6
2-[(2,3-Dimethylphenyl) amino] benzoic acid	–	–	–	–	–	–7.7
1-Benzyl-4-[(5,6-dimethoxy-1-indanon-2-yl) methyl] piperidine I	–	–	–7.6	–	–	–

Among the 32 selected hits, each compound was found to possess a docking score above or equal to -6.5 for one or the other target protein. For the target proteins AChE, MMP-1, Keap1, and COX-2, maximum docking scores were reported for palythenic acid (−8.2), mycosporine-ornithine (−7.0), mycosporine-glutamine (−8.4), and porphyra-334 (−7.9), respectively. However, minimum scores were obtained by mycosporine-taurine (−5.7, AChE), aplysiapalythine-B (−5.9, 3SHI), asterina (−5.9, 1U6D), and mycosporine-glumicol (−5.8, 5IKR).

3.3. Pharmacokinetics analysis and toxicity risk assessment

Assessment of a chemical's suitability for human use involves the analysis of its pharmacokinetic behavior and predicted toxicity. In this study, drug-likeness and ADME parameters of MAAs are evaluated using the SwissADME, a web-based tool. Table 3 summarizes the pharmacological and drug-likeness parameters of the compounds under study. The physicochemical and drug-likeness evaluation of MAAs and their derivatives was carried out using computational analysis tools. Parameters such as MW, partition coefficient (LogP), HBA and HBD, topological polar surface area (TPSA), and solubility were analyzed to predict bioavailability, permeability, and overall drug-likeness were estimated [28, 29].

The MWs of the analyzed MAAs ranged from approximately 239 to 374 Da, which is within the acceptable range (<500 Da) for orally active compounds according to Lipinski's rule of five. This suggests that most MAAs possess a favorable molecular size for drug absorption and distribution. Compound mycosporine-glutamic acid-glycine showed slightly higher MW and was found to violate more than one of Lipinski's rule. Therefore, the compound mycosporine-glutamic acid-glycine was eliminated at this stage. Although several MAAs demonstrated favorable binding affinity toward acetylcholinesterase (AChE), it is important to note that most compounds were predicted to exhibit low BBB permeability according to SwissADME analysis. This suggests that direct central nervous system (CNS) neuroprotective effects may be limited without structural modification or advanced delivery strategies. Therefore, the neuroprotective relevance proposed in this study should be interpreted as a computational indication of target interaction potential rather than confirmed CNS therapeutic activity. Future *in vitro* enzyme inhibition studies and formulation-based approaches would be necessary to validate and enhance brain accessibility.

The LogP values of all compounds were negative, indicating a hydrophilic nature. These values suggest that MAAs are more soluble in aqueous media than in lipophilic environments, consistent with their natural role as water-soluble UV protective molecules. Although high hydrophilicity may limit passive membrane diffusion, it enhances systemic solubility, which is advantageous for topical and oral formulations. The high solubility ratings (mostly "very soluble" or "highly soluble") further confirm their excellent aqueous compatibility, supporting their use in cosmetic or dermatological applications.

Hydrogen bonding is a key determinant in ligand-receptor interactions and permeability. The MAAs exhibited HBA values ranging from 4 to 9 and HBD values from 3 to 8, both within acceptable ranges for drug-like compounds. Compounds with moderate numbers of HBA and HBD are likely to show good binding affinity to biological targets while maintaining adequate permeability. Similarly, TPSA values ranged between 100 and 160, suggesting strong polarity. Although higher TPSA values (>140) may reduce BBB penetration, they enhance hydrophilicity and reduce nonspecific toxicity. Accordingly, all compounds were predicted to have no BBB permeability, which is desirable for non-neuroactive agents.

The Lipinski rule violations were minimal (mostly zero), and the predicted bioavailability scores were consistently around 0.55, suggesting that MAAs generally fulfill key criteria for oral bioavailability. Moreover, PAINS (pan-assay interference compounds) alerts were absent for all compounds, indicating low

Table 3. Physicochemical properties of the active compounds in accordance with the rule of drug-likeness. MW: molecular weight; HBA: hydrogen bond acceptor; HBD: hydrogen bond donor; AMR: atom molar refractivity; TPSA: topological polar surface area; nRB: number of rotatable bonds; BBB: blood–brain barrier; GI: gastrointestinal; PAINS: pan-assay interference compounds (selected hits for further assessment are mentioned in bold)

Ligands	MW (g/mol)	Log P	HBA	HBD	AMR	TPSA	AlogS	Solubility	nRB	No. of violations of Lipinski rule	LogKp	Bioavail -ability	BBB	GI absorption	PAINS alert
Aplysiapalythine-A	259.28	–1.29	5	5	64.78	112.99	–0.59	Very soluble	5	0	–8.8	0.55	No	Low	0
Aplysiapalythine-B	275.32	–1.92	7	5	68	111.05	2.16	Highly soluble	7	0	–10.75	0.55	No	High	0
Aplysiapalythine -C	303.33	–1.45	6	6	75.55	133.22	–0.85	Very soluble	7	1	–9.17	0.55	No	Low	0
Asterina-330	288.30	–0.92	7	5	70.08	131.61	–0.20	Very soluble	7	0	–9.45	0.56	No	Low	0
Deoxygadusol	188.18	–0.53	5	3	43.2	86.99	0.07	Highly soluble	2	0	–8.44	0.56	No	High	0
Euhalothece-362	330.33	–0.78	8	6	80.79	151.84	–1.36	Very soluble	7	1	–9.26	0.11	No	Low	0
Gadusol	204.18	–1.2	6	4	44.36	107.22	0.23	Highly soluble	2	0	–8.94	0.56	No	High	0
Mycosporine-Methylamine-serine	258.87	–0.62	6	4	64.11	114.08	–0.66	Very soluble	6	0	–8.76	0.56	No	High	0
Mycosporine-serinol	261.67	–1.31	6	5	61.7	119.25	0.39	Highly soluble	6	0	–9.57	0.55	No	Low	0
Mycosporine-taurine	295.31	–1.34	7	4	64.58	141.54	–0.83	Very soluble	6	0	–9.26	0.56	No	Low	0
Mycosporine-2-glycine	302.28	–1.47	8	5	70.69	148.68	–1.02	Very soluble	7	0	–9.27	0.56	No	Low	0
Mycosporine-GABA	273.28	–0.34	6	4	65.43	116.09	–0.73	Very soluble	7	0	–8.83	0.56	No	Low	0
Mycosporine-glutamicol	303.31	–0.82	7	5	71.4	136.32	–0.51	Very soluble	8	0	–9.45	0.56	No	Low	0
Mycosporine-glutamine	316.31	–1.88	7	5	73.14	159.18	–0.58	Very soluble	8	0	–9.81	0.11	No	Low	0
Mycosporine-glycine-valine	344.36	–0.56	8	5	85.11	148.68	–2.43	Soluble	8	0	–8.56	0.56	No	Low	0
Mycosporine-glycine	245.23	–1.33	6	4	55.82	116.09	–0.46	Very soluble	5	0	–8.84	0.56	No	High	0
Mycosporine –glutamic acid-glycine	374.34	–1.64	10	6	86.88	185.95	–1.69	Very soluble	10	2	–9.79	0.11	No	Low	0
Mycosporine-hydroxyglutamicol	319.31	–1.52	8	6	72.56	156.55	0.07	Highly soluble	8	1	–10.24	0.11	No	Low	0
Mycosporine-lysine	316.35	–1.35	7	5	77.75	142.11	1.18	Highly soluble	9	0	–10.77	0.55	No	Low	0
Mycosporine-methylamine-threonine	302.32	–1.11	7	5	74.88	131.61	–0.75	Very soluble	6	0	–9.22	0.56	No	Low	0
Mycosporine-ornithine	302.32	–1.72	7	5	72.94	142.11	1.55	Highly soluble	8	0	–10.94	0.55	No	Low	0
Mycosporine-glycine-alanine	316.31	–1.18	8	5	75.49	148.68	–1.44	Very soluble	7	0	–9.07	0.56	No	Low	0
Palythine-serine	274.27	–1.3	7	5	65.18	145.6	–0.01	Very soluble	5	0	–9.75	0.56	No	Low	0
Palythene	284.31	0.18	6	4	73.25	111.38	–1.4	Very soluble	6	0	–8.37	0.56	No	High	0
Palythenic acid	328.32	–0.89	8	5	79.83	148.68	–1.92	Very soluble	7	0	–8.82	0.56	No	Low	0
Palythine	244.24	–0.95	6	4	59.21	125.37	–0.26	Very soluble	4	0	–9.1	0.56	No	High	0
Palythene-threonine	288.3	–1.04	7	5	69.98	145.6	–0.46	Very soluble	5	0	–9.53	0.56	No	Low	0
Palythinol	302.32	–0.67	7	5	74.88	131.61	–0.82	Very soluble	7	0	–9.17	0.56	No	Low	0
Porphyra-334	364.33	–1.7	9	6	81.46	168.91	–1.22	Very soluble	8	1	–9.7	0.11	No	Low	0
Usujirene	284.31	0.18	6	4	73.25	111.38	–1.4	Very soluble	6	0	–8.37	0.56	No	High	0
Shinorine	332.31	–0.68	9	6	76.66	168.91	–0.77	Very soluble	8	1	–9.92	0.11	No	Low	0

likelihood of assay interference and high reliability as screening hits. The GI absorption was predicted as low for most MAAs, which can be attributed to their hydrophilic nature and high TPSA values. However, this characteristic may favor topical formulations where high solubility and UV absorption are critical. Figure 2 represents the BOILED-egg predictive plot, which displays the distribution of compounds within the yellow region (BBB permeable) and white region (HIA: high intestinal absorption). Blue circles represent P-glycoprotein substrates (PGP+), while red circles denote non-substrates (PGP–). Most compounds fall within the HIA zone, indicating good intestinal absorption, whereas only a few lie within the BBB region, indicating a restricted capacity for BBB penetration. The separation between PGP+ and PGP– molecules reflects differences in efflux susceptibility, which is important for assessing CNS drug-likeness and therapeutic potential [30].

All the shortlisted compounds that satisfied Lipinski's rule of five were further assessed for their toxicity profiles using the Osiris Property Explorer. This tool evaluates the presence of structural fragments that are commonly associated with toxic effects, offering predictive insight into potential safety risks. The analysis revealed that none of the evaluated molecules showed any indication of mutagenic, tumorigenic, irritant, or reproductive toxicity, as summarized in Table 4. In addition, every compound exhibited favorable DS values, varying between 0.45 and 0.83, reflecting their strong overall drug-likeness. However, for aplysiapalythine-A, aplysiapalythine-B, and aplysiapalythine-C, reliable toxicity results could not be generated, and consequently, these molecules were excluded from further consideration. The remaining compounds demonstrated desirable pharmacokinetic properties, supporting their potential as viable and promising candidates for interaction with the selected target proteins.

3.4. Oral toxicity assessment

Twenty-two MAAs showed no predicted AMES toxicity, hepatotoxicity, or skin sensitization, indicating a generally favorable safety profile (Table 5). In addition, acute oral toxicity (LD50) and chronic oral toxicity (LOAEL) values were estimated in rats for all selected compounds. This evaluation provides a deeper understanding of their potential biological effects and mechanisms of action.

3.5. Protein-ligand interaction study and visualization

The amino acid residues contributing to protein–ligand binding in the complexes formed by the selected top-ranked ligands with the target proteins are depicted in Figure 3. Three compounds with the highest docking scores for each receptor and demonstrating favorable ADME and toxicity profiles were selected for detailed interaction analysis. The 3D interaction profiles of the docked complexes were visualized using PyMOL along with BIOVIA Discovery Studio 2021 [31, 32]. The contributing amino acid residues of the target protein with each ligand were identified through BIOVIA Discovery Studio 2021. Table 6 highlights the top-ranking compounds, presenting their 2D structures, the predicted interacting residues, the total number of hydrogen bonds formed, and the corresponding bond lengths. It is important to emphasize that molecular docking provides a theoretical estimation of binding affinity and

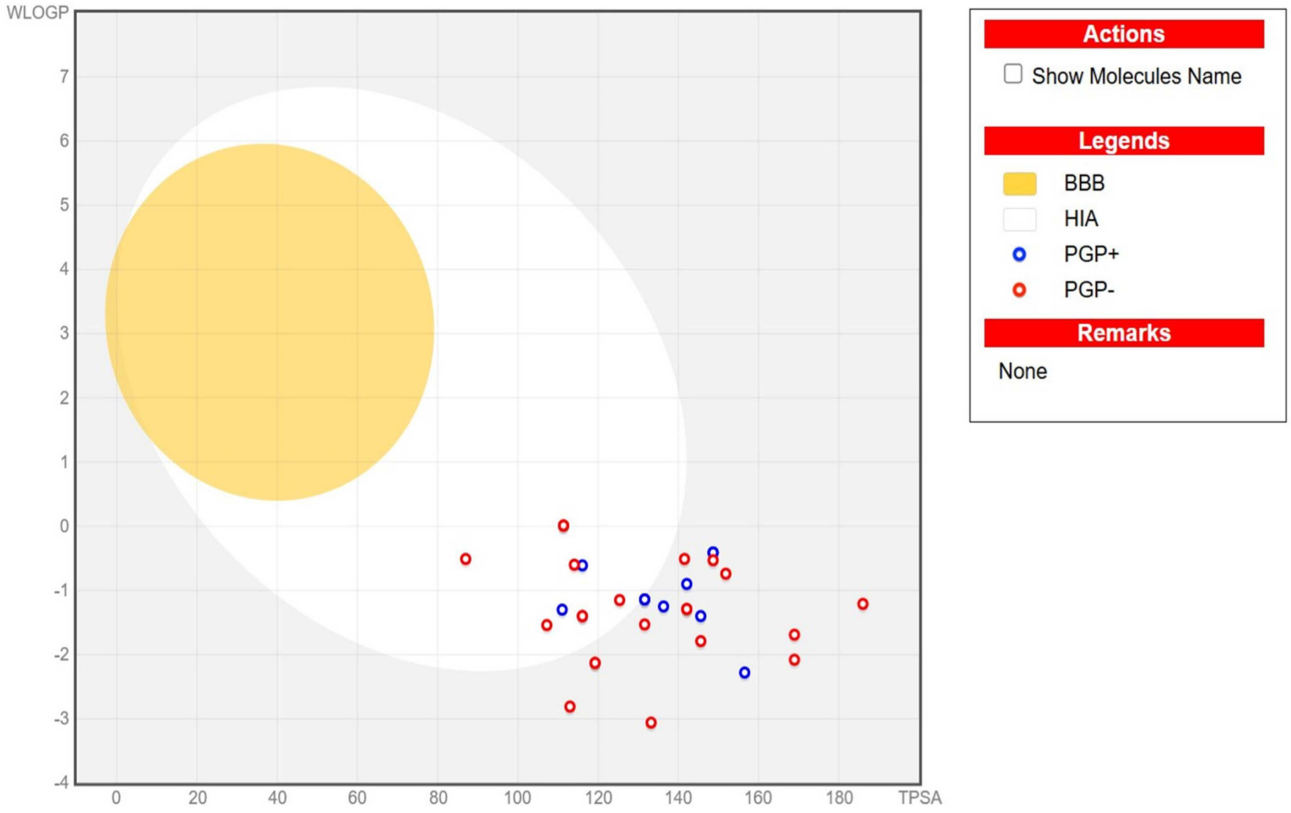

Figure 2. BOILED-Egg predictive model illustrating gastrointestinal absorption and blood–brain barrier permeation of the selected ligands based on WLOGP versus TPSA parameters

Table 4. Drug-likeliness and toxicity profile of selected compounds (MAAs) using OSIRIS Property Explorer (selected hits for further assessment are mentioned in bold)

Ligands	Mutagenic	Tumorigenic	Irritant	Reproductive effect	Solubility	Drug-likeness	Drug score
Aplysiapalythine-A	–	–	–	–	–	–	–
Aplysiapalythine-B	–	–	–	–	–	–	–
Aplysiapalythine -C	–	–	–	–	–	–	–
Asterina-330	No	No	No	No	–0.38	–1.8	0.55
Deoxygadusol	No	No	No	No	–0.77	–2.08	0.54
Euhalothece-362	No	No	No	No	–1.19	–0.08	0.69
Gadusol	No	No	No	No	–0.37	–1.59	0.57
Mycosporine-methylamine-serine	No	No	No	No	0.65	–2.49	0.52
Mycosporine-serinol	No	No	No	No	–0.42	–1.7	0.56
Mycosporine-taurine	No	No	No	No	–0.28	–8.0	0.48
Mycosporine-2-glycine	No	No	No	No	–0.37	–3.11	0.5
Mycosporine-GABA	No	No	No	No	–1.07	–1.11	0.6
Mycosporine-glutamicol	No	No	No	No	–0.94	–1.44	0.57
Mycosporine-glutamine	No	No	No	No	–1.0	–2.0	0.5
Mycosporine-glycine-valine	No	No	No	No	–1.17	–2.88	0.49
Mycosporine-glycine	No	No	No	No	–0.53	–3.25	0.5
Mycosporine-hydroxyglutamicol	No	No	No	No	–0.55	1.13	0.83
Mycosporine-lysine	No	No	No	No	–1.29	–17.06	0.47
Mycosporine-methylamine-threonine	No	No	No	No	–0.84	–0.42	0.66
Mycosporine-ornithine	No	No	No	No	–1.02	–12.98	0.42
Mycosporine-glycine-alanine	No	No	No	No	–0.74	–0.16	0.69
Palythine-serine	No	No	No	No	–0.55	–0.5	0.66
Palythene	No	No	No	No	–1.38	–3.28	0.49
Palythenic acid	No	No	No	No	–1.11	–2.05	0.52
Palythine	No	No	No	No	–0.67	–2.85	0.51
Palythene-threonine	No	No	No	No	–0.92	–1.1	0.6
Palythinol	No	No	No	No	–0.76	–2.13	0.53
Porphyra-334	No	No	No	No	–0.61	–1.36	0.56
Usujirene	No	No	No	No	–1.38	–3.28	0.49
Shinorine	No	No	No	No	–0.24	–0.54	0.64

Table 5. Computational estimation of oral toxicity (LD50) of screened MAAs (selected hits for further assessment are mentioned in bold)

Ligands	Toxicity (AMES)	Tolerated dose (log/mg/kg/day)	Oral rat acute toxicity (LD50) mol/kg	Oral rat chronic toxicity (LOAEL) (log/mg/kg_bw/day)	Hepatotoxicity	Skin sensitization
Asterina-330	No	1.155	1.776	2.491	No	No
Deoxygadusol	No	1.823	1.532	2.531	No	No
Euhalothece-362	No	1.072	2.059	2.171	Yes	No
Gadusol	No	2.038	1.531	3.036	No	No
Mycosporine-methylamine-serine	No	1.245	1.821	2.957	No	No
Mycosporine-serinol	No	1.695	2.031	2.604	No	No
Mycosporine-taurine	No	1.084	1.712	2.773	No	No
Mycosporine-2-glycine	No	1.084	1.863	2.703	No	No
Mycosporine-GABA	No	0.834	1.713	2.465	No	No
Mycosporine-glutamicol	No	1.007	1.772	2.629	No	No
Mycosporine-Glutamine	No	1.512	1.665	2.622	No	No
Mycosporine-glycine	No	1.673	1.56	2.716	No	No
Mycosporine-hydroxyglutamicol	No	1.268	1.844	3.028	No	No
Mycosporine-lysine	No	1.092	2.237	2.518	No	No
Mycosporine-methylamine-threonine	No	1.143	1.895	2.367	No	No
Mycosporine-ornithine	No	1.126	2.239	2.468	No	No
Mycosporine-alanine	No	1.281	1.596	2.473	No	No
Mycosporine-glycine-valine	No	0.355	1.638	2.62	Yes	No
Palythine-serine	No	1.832	1.522	2.743	No	No
Palythenic acid	No	0.789	1.732	2.543	Yes	No
Palythene	No	0.865	1.811	2.319	Yes	No
Palythine	No	1.259	1.698	2.59	No	No
Palythine-threonine	No	1.289	1.706	2.502	No	No
Palythine-serine	No	1.832	1.522	2.743	No	No
Palythinol	Yes	1.04	2.482	3.294	No	No
Porphyra-334	No	1.002	1.847	2.579	Yes	No
Usujirene	No	0.865	1.811	2.319	No	No
Shinorine	No	1.364	1.791	2.798	No	No

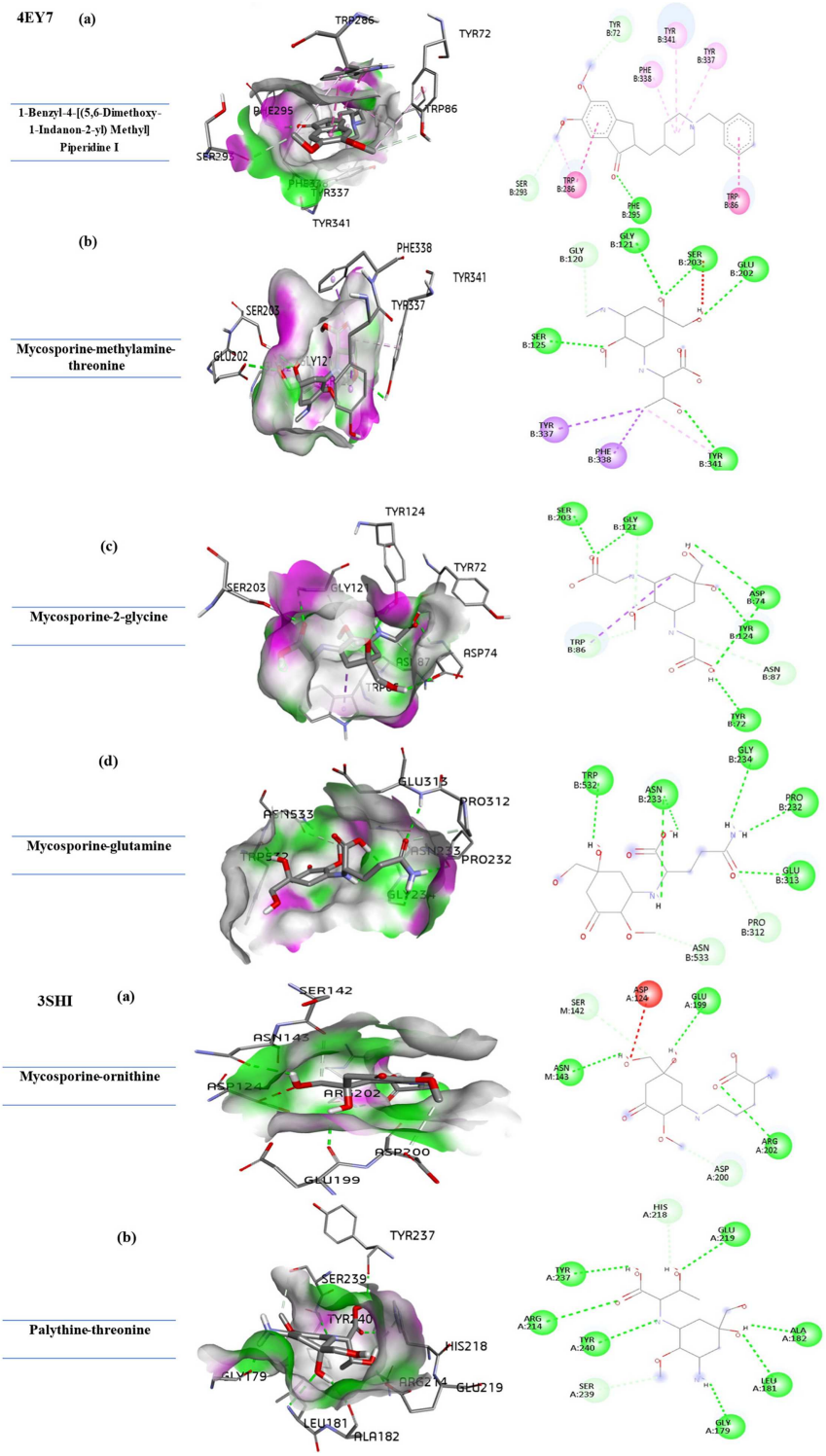
4EY7
(a)
1-Benzyl-4-[(5,6-Dimethoxy-1-Indanon-2-yl) Methyl] Piperidine I
TRP286
TYR72
TYR86
SER293
PHE295
TYR337
TYR341
PHE338
(b)
Mycosporine-methylamine-threonine
PHE338
TYR341
TYR337
SER203
GLU202
(c)
Mycosporine-2-glycine
TYR124
TYR72
SER203
ASP74
(d)
Mycosporine-glutamine
GLU313
PRO312
ASN533
TRP532
PRO232
3SHI
(a)
Mycosporine-ornithine
SER142
ASN143
ASP124
ARG202
ASP200
GLU199
(b)
Palythine-threonine
TYR237
SER239
TYR240
HIS218
GLY179
ARG214
GLU219
LEU181
ALA182

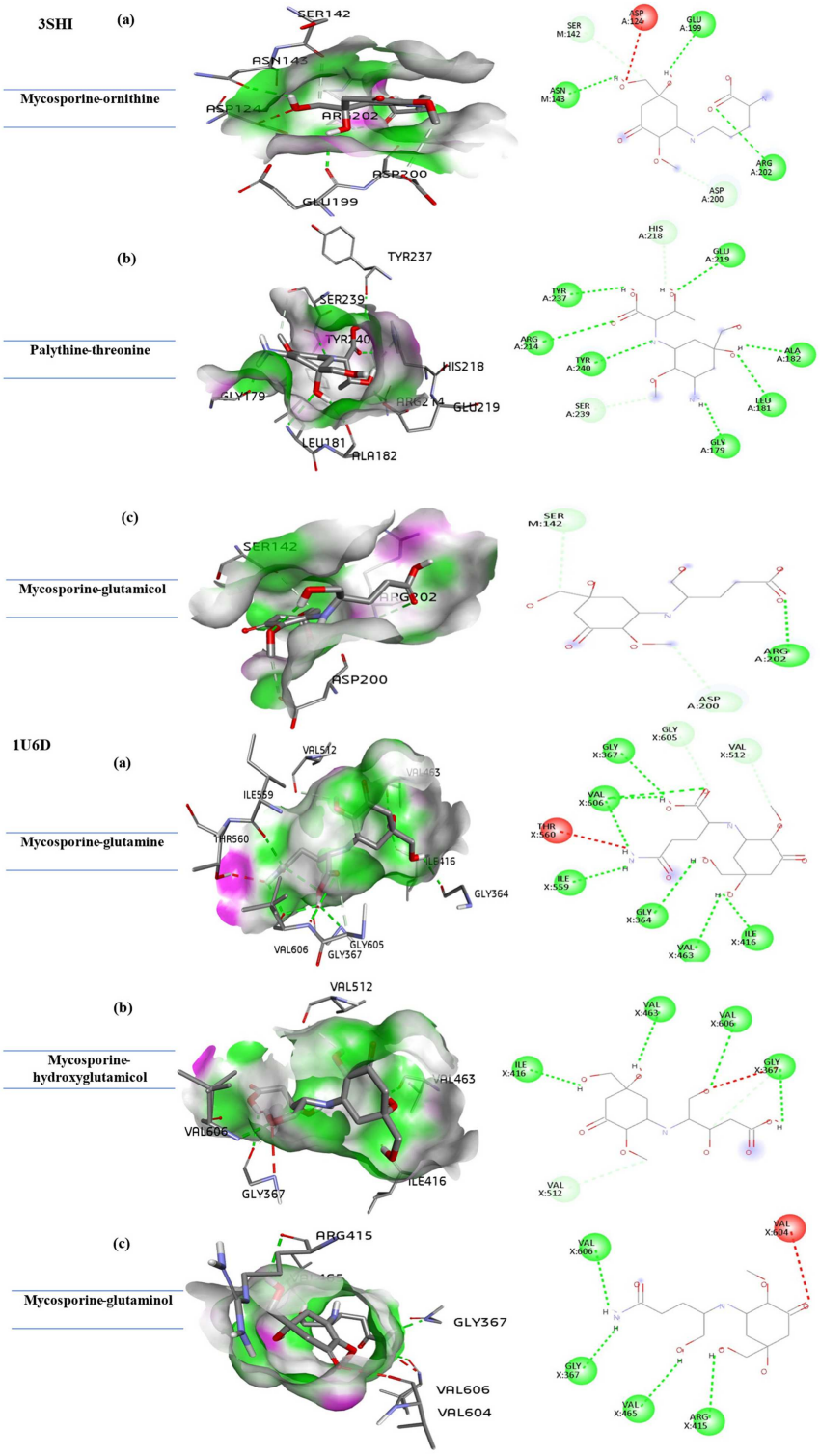
3SHI
(a)
Mycosporine-ornithine
SER142
ASN143
ASP124
ARG202
ASP200
GLU199
(b)
Palythine-threonine
TYR237
SER239
TYR240
HIS218
GLY179
ARG214
GLU219
LEU181
ALA182
(c)
Mycosporine-glutamicol
SER142
ARG202
ASP200
1U6D
(a)
Mycosporine-glutamine
VAL512
ILE559
THR560
ILE416
GLY364
VAL606
GLY605
GLY367
(b)
Mycosporine-hydroxyglutamicol
VAL512
VAL463
VAL606
ILE416
GLY367
(c)
Mycosporine-glutaminol
ARG415
GLY367
VAL606
VAL604

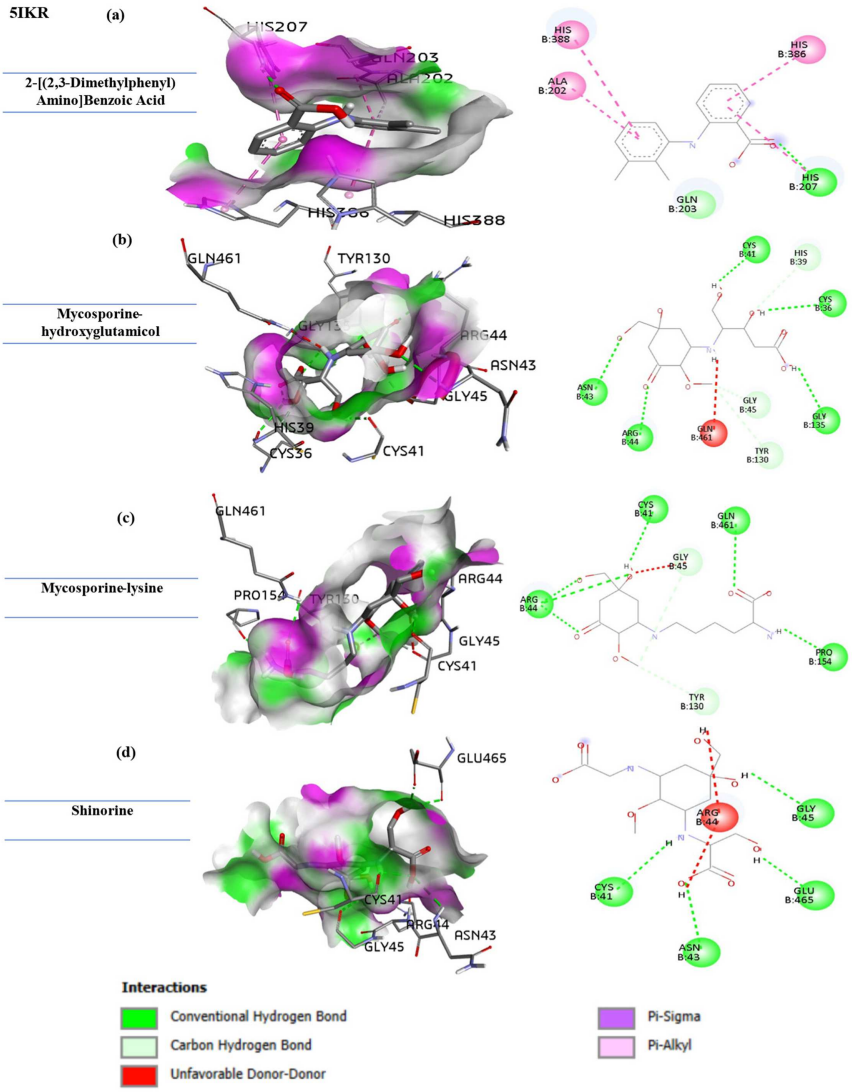

Figure 3. Representative 3D binding pose and 2D interaction diagram of top-ranked MAAs within the active site of each target protein. Hydrogen bonds are shown as green dashed lines

interaction patterns between ligands and target proteins. While favorable docking scores suggest potential molecular compatibility, they do not directly measure enzymatic inhibition, pharmacodynamic response, or *in vivo* therapeutic efficacy. Similarly, ADME and toxicity analyses represent computational predictions rather than experimentally verified pharmacokinetic properties. Therefore, the present findings should be interpreted as preliminary *in silico* evidence of multitarget binding potential, requiring subsequent biochemical assays, molecular dynamics simulations, and biological validation studies to establish functional activity.

3.6. Comparative multitarget binding analysis

To avoid overinterpretation based on individual docking scores, a comparative multitarget analysis was performed. Compounds were evaluated based on the number of targets for which they exhibited binding affinities ≤ –6.5 kcal/mol. Several MAAs, including mycosporine-glutamine and shinorine, demonstrated favorable binding across three distinct targets, suggesting broader multitarget compatibility. Importantly, no compound displayed uniformly high affinity across all four proteins, indicating that the observed interactions reflect differential target compatibility rather than universal potency. This pattern supports the interpretation of MAAs as structurally adaptable ligands rather than definitive multitarget inhibitors.

4. Limitations of the Study

While the present investigation provides a comprehensive computational assessment, several limitations must be acknowledged. Molecular docking predicts static binding conformations and approximate affinity values but does not account for protein flexibility, solvent dynamics, entropy contributions, or kinetic inhibition constants. Additionally, ADME and toxicity profiles represent *in silico* estimations derived from predictive models rather than experimental validation. The absence of molecular dynamics simulations further limits the evaluation of binding stability over time. Therefore, the present findings should be interpreted as hypothesis-generating rather than confirmatory. Experimental enzyme inhibition assays, cellular validation, and dynamic simulation studies are necessary to substantiate the proposed interactions.

Table 6. 2D interaction profiles illustrating binding residues and measured bond lengths between the target protein and the top-scoring ligands, generated using BIOVIA Discovery Studio

Target protein	Ligand with top 3 dock score	Docking score	No of conventional hydrogen bonds	Ligand–residue interaction (bond length in Å)	No of carbon–hydrogen bond	Ligand–residue interaction (bond length in Å)
4EY7	Mycosporine-methylamine-threonine	–8.1	5	Gly-121(2.87), Ser-125(2.02), Glu-202(3.18), Ser-203(2.66), Tyr-341(2.94)	1	Gly-120(3.48)
	Mycosporine-2-glycine	–8.0	6	Tyr-72(2.45), Asp-74(2.65), Asp-74(2.65), Gly-121(2.75), Tyr-124(2.58), Ser-203(1.96)	3	Trp-86(3.32), Asn-87(3.28), Gly-121(3.31)
	Mycosporine-glutamine	–8.0	6	Pro-232(2.72), Asn-233(1.98), Asn-233(2.36), Gly-234(2.76), Glu-313(2.47), Trp-532(2.18)	2	Pro-312(3.55), Asn-533(3.66)
	1-Benzyl-4-[(5,6-dimethoxy-1-indanon-2-yl) methyl] piperidine I	–7.6	1	Phe-295(1.80)	–	–
	Mycosporine-ornithine	–7.0	3	Asn-143(2.33), Glu-199(2.53), Arg-202(2.95)	2	Ser-142(3.60), Asp-200(3.73)
3SHI	Palythine-threonine	–6.9	7	Gly-179(1.96), Leu-181(1.96), Ala-182(2.19), Glu-219(2.3), Arg-214(2.75), Tyr-237(2.14), Tyr-240(2.95)	2	His-218(3.06), Ser-239(3.72)
	Mycosporine-glutamicol	–6.9	2	Arg-202(2.65), Arg-202(3.09)	2	Ser-142(3.58), Asp-200(3.54)
1U6D	Mycosporine-glutamine	–8.4	8	Gly-364(2.34), Gly-367(2.59), Ile-416(2.15), Val-463(2.79), Ile-559(2.32), Val-606(2.56), Val-606(2.49), Val-606(3.31)	2	Val-512(3.67), Gly-605(3.38)
	Mycosporine-hydroxyglutamicol	–8.2	4	Gly-367(2.28), Ile-416(1.84), Val-463(3.59), Val-606(3.18)	2	Gly-367(3.60), Val-512(3.64)
	Mycosporine-glutaminol	–8.0	4	Gly-367(2.18), Arg-415(2.64), Val-465(2.5), Val -606(2.59)	–	–
5IKR	Mycosporine-hydroxyglutamicol	–7.7	5	Cys-36(2.54), Cys-41(2.35), Asn-43(2.7), Arg-44(2.15), Gly-135(2.83)	3	His-39(3.38), Gly-35(3.33), Tyr-130(3.47)
	Mycosporine-lysine	–7.7	6	Cys-41(2.25), Arg-44(2.74), Arg-44(2.30), Arg-44(1.95), Pro-154(2.1), Gln-461(2.81)	2	Gly-45(3.18), Tyr-130(3.23)
	Shinorine	–7.6	5	Cys-41(2.69), Asn-43(2.92), Gly-45(2.63), Glu-465(2.06), Glu-465(3.09)	–	–
	2-[(2,3-Dimethylphenyl) amino] benzoic acid	–7.7	1	His-207(2.33)	–	–

5. Conclusions

The present study provides an integrative *in silico* evaluation of MAAs against multiple biologically relevant targets associated with aging, oxidative stress, and inflammation. The combined docking, pharmacokinetic, and toxicity analyses suggest that several MAAs possess favorable binding characteristics and acceptable safety profiles, particularly for dermatological and antioxidant-related applications. However, it is crucial to distinguish computational predictions from experimentally validated therapeutic effects. While the docking results indicate multitarget binding potential, they do not confirm biological efficacy or clinical applicability. Furthermore, predicted low BBB permeability limits direct inference of central neuroprotective action without further structural optimization or delivery strategies. Overall, this study establishes a computational foundation for future experimental investigations aimed at validating the pharmacological potential of MAAs beyond their established photoprotective role.

Acknowledgment

Varsha K. Singh (09/0013 (12862)/2021-EMR-1) is thankful to the Council of Scientific & Industrial Research, New Delhi, India, for financial assistance in the form of SRF. The incentive grant received from IoE (Scheme no. 6031), Banaras Hindu University, Varanasi, India, to Rajeshwar P. Sinha is highly acknowledged.

Ethical Statement

This study does not involve any data derived from human or animal subjects. No experiments or procedures involving humans or animals were conducted by the authors. Therefore, ethical approval from any institutional ethics committee was not required for this work. The study is based solely on computational analysis/review of previously published literature, and all sources have been appropriately cited in accordance with standard academic practices.

Conflicts of Interest

The authors declare that they have no conflicts of interest to this work.

Data Availability Statement

The data that support the findings of this study are presented in the form of tables and figures within the MS.

Author Contribution Statement

Varsha K. Singh: Methodology, Software, Formal analysis, Investigation, Data curation, Writing – original draft, Writing – review & editing, Visualization. **Niharika Sahu:** Methodology, Formal analysis, Investigation, Data curation, Writing – original draft, Writing – review & editing, Visualization. **Rajeshwar P. Sinha:** Conceptualization, Validation, Resources, Supervision, Project administration.

References

[1] Geraldes, V., & Pinto, E. (2021). Mycosporine-like amino acids (MAAs): Biology, chemistry and identification features. *Pharmaceuticals (Basel)*, *14*(1), 63. https://doi.org/10.3390/ph14010063

[2] Yamamoto, R., Toriumi, S., Kawagoe, C., Saburi, W., Kishimura, H., & Kumagai, Y. (2024). Extraction and antioxidant capacity of mycosporine-like amino acids from red algae in Japan. *Bioscience, Biotechnology, and Biochemistry*, *88*(7), 830–838. https://doi.org/10.1093/bbb/zbae051

[3] Singh, A., Čížková, M., Bišová, K., & Vítová, M. (2021). Exploring mycosporine-like amino acids (MAAs) as safe and natural protective agents against UV-induced skin damage. *Antioxidants (Basel)*, *10*(5), 683. https://doi.org/10.3390/antiox10050683

[4] Punchakara, A., Prajapat, G., Bairwa, H. K., Jain, S., & Agrawal, A. (2023). Applications of mycosporine-like amino acids beyond photoprotection. *Applied and Environmental Microbiology*, *89*(11), e0074023. https://doi.org/10.1128/aem.00740-23

[5] Rosic, N. N. (2019). Mycosporine-like amino acids: Making the foundation for organic personalised sunscreens. *Marine Drugs*, *17*(11), 638. https://doi.org/10.3390/md17110638

[6] Singh, V. K., Jha, S., Rana, P., Mishra, S., Kumari, N., Singh, S. C., . . . , & Sinha, R. P. (2023). Resilience and mitigation strategies of cyanobacteria under ultraviolet radiation stress. *International Journal of Molecular Sciences*, *24*(15), 12381. https://doi.org/10.3390/ijms241512381

[7] Sen, S., & Mallick, N. (2021). Mycosporine-like amino acids: Algal metabolites shaping the safety and sustainability profiles of commercial sunscreens. *Algal Research*, *58*, 102425. https://doi.org/10.1016/j.algal.2021.102425

[8] Cheung, J., Rudolph, M. J., Burshteyn, F., Cassidy, M. S., Gary, E. N., Love, J., . . . , & Height, J. J. (2012). Structures of human acetylcholinesterase in complex with pharmacologically important ligands. *Journal of Medicinal Chemistry*, *55*(22), 10282–10286. https://doi.org/10.1021/jm300871x

[9] Wu, J., Wang, L., Yang, S., Pei, S., Liu, T., Zhou, Q., . . . , & Wu, Q. (2025). In-depth analysis of acetylcholinesterase: Recent advances in structure, function and assays. *Biochemical Engineering Journal*, *226*, 109974. https://doi.org/10.1016/j.bej.2025.109974

[10] Bertini, I., Calderone, V., Cerofolini, L., Fragai, M., Geraldes, C.F., Hermann, P., . . . , & Teixeira, J. M. (2012). The catalytic domain of MMP-1 studied through tagged lanthanides. *FEBS Letters*, *586*(5), 557–567. https://doi.org/10.1016/j.febslet.2011.09.020

[11] Van Doren, S. R. (2015). Matrix metalloproteinase interactions with collagen and elastin. *Matrix Biology*, *4*(*4-46*), 224–31. https://doi.org/10.1016/j.matbio.2015.01.005

[12] Cabral-Pacheco, G. A., Garza-Veloz, I., Castruita-De la, Rosa., C, Ramirez-Acuña., M, J., Perez-Romero, B. A., Guerrero-Rodriguez, J. F., Martinez-Fierro, M. L., . . . , & Martinez-Fierro, M. L. (2020). The roles of matrix metalloproteinases and their inhibitors in human diseases. *International Journal of Molecular Sciences*, *21*(24), 9739. https://doi.org/10.3390/ijms21249739

[13] Li, X., Zhang, D., Hannink, M., & Beamer, L. J. (2004). Crystal structure of the Kelch domain of human Keap1*. *Journal of Biological Chemistry*, *279*(52), 54750–54758. https://doi.org/10.1074/jbc.m410073200

[14] Mann, G. E., & Forman, H. J. (2015). Introduction to special issue on'Nrf2 regulated redox signaling and metabolism in physiology and medicine. *Free Radical Biology &*

Medicine, *88*, 91–92. https://doi.org/10.1016/j.freeradbiomed.2015.08.002

[15] Orlando, B. J., & Malkowski, M. G. (2016). Substrate-selective inhibition of cyclooxygeanse-2 by fenamic acid derivatives is dependent on peroxide tone. *Journal of Biological Chemistry*, *291*(29), 15069–15081. https://doi.org/10.1074/jbc.m116.725713

[16] Rahman, M. M., Junaid, M., Hosen, S. Z., Mostafa, M., Liu, L., & Benkendorff, K. (2021). Mollusc-derived brominated indoles for the selective inhibition of cyclooxygenase: A computational expedition. *Molecules*, *26*(21), 6538. https://doi.org/10.3390/molecules26216538

[17] Janakiramulu, P., & Mamidala, E. (2025). Molecular Docking and dynamic simulation analysis of flavonoid derivatives as COX-2 inhibitors. *In Silico Pharmacology*, *13*, 59. https://doi.org/10.1007/s40203-025-00349-x

[18] Singh, V. K., Sahu, N., Kesheri, M., Kanchan, S., Kumar, A., & Sinha, R. P. (2025). Screening mycosporine-like amino acids (MAAs) as potential inhibitors of a malaria-associated cysteine protease falcipain-2. *Computers in Biology and Medicine*, *196*, 110815. https://doi.org/10.1016/j.compbiomed.2025.110815

[19] Rosenberg, A. A., Marx, A., & Bronstein, A. M. (2024). A dataset of alternately located segments in protein crystal structures. *Science Data*, *11*, 783. https://doi.org/10.1038/s41597-024-03595-4

[20] Tian, W., Chen, C., Lei, X., Zhao, J., & Liang, J. (2018). CASTp 3.0: Computed atlas of surface topography of proteins. *Nucleic Acids Research*, *46*(W1), W363–W367. https://doi.org/10.1093/nar/gky473

[21] Kirkwood, J., Hargreaves, D., O'Keefe, S., & Wilson, J. (2015). Analysis of crystallization data in the Protein Data Bank. *Acta Crystallographic F: Structural Biology Communications*, *71*, 1228–1234. https://doi.org/10.1107/S2053230X15014892

[22] Che, X., Liu, Q., & Zhang, L. (2023). An accurate and universal protein-small molecule batch docking solution using Autodock Vina. *Results in Engineering*, *19*, 101335. https://doi.org/10.1016/j.rineng.2023.101335

[23] Sastry, G. M., Adzhigirey, M., Day, T., Annabhimoju, R., & Sherman, W. (2013). Protein and ligand preparation: Parameters, protocols, and influence on virtual screening enrichments. *Journal of Computer Aided Molecular Design*, *27*(3), 221–34. https://doi.org/10.1007/s10822-013-9644-8

[24] Daina, A., Michielin, O., & Zoete, V. (2017). SwissADME: A free web tool to evaluate pharmacokinetics, drug-likeness and medicinal chemistry friendliness of small molecules. *Scientific Reports*, *7*(1), 42717. https://doi.org/10.1038/srep42717

[25] Arango, J. P. B., Rodriguez, D. Y. M., Cruz, S. L., & Ocampo, G. T. (2025). In silico evaluation of pharmacokinetic properties and molecular docking for the identification of potential anticancer compounds. *Computational Biology and Chemistry*, *120*(1), 108626. https://doi.org/10.1016/j.compbiolchem.2025.108626

[26] Pires, D. E., Kaminskas, L. M., & Ascher, D. B. (2018). *Prediction and optimization of pharmacokinetic and toxicity properties of the ligand In Computational drug discovery and design* (pp. 271–284). Springer New York. https://doi.org/10.1007/978-1-4939-7756-7

[27] Kaavin, K., Naresh, D., Yogeshkumar, M. R., Prakash, M. K., Janarthanan, S., Krishnan, M. M., & Malathi, M. (2024). In-silico DFT studies and molecular docking evaluation of benzimidazo methoxy quinoline-2-one ligand and its Co, Ni, Cu and Zn complexes as potential inhibitors of Bcl-2, Caspase-3, EGFR, mTOR, and PI3K, cancer-causing proteins. *Chemical Physics Impact*, *8*, 100418. https://doi.org/10.1016/j.chphi.2023.100418

[28] Gupta, A., Sahu, N., Singh, A. P., Singh, V. K., Singh, S. C., Upadhye, V. J., . . . , & Sinha, R.P. (2022). Exploration of novel lichen compounds as inhibitors of SARS-CoV-2 Mpro: Ligand-based design, molecular dynamics, and ADMET analyses. *Applied Biochemistry and Biotechnology*, *194*(12), 6386–6406. https://doi.org/10.1007/s12010-022-04103-3

[29] Ma, S., McGann, M., & Enyedy, I. J. (2021). The influence of calculated physicochemical properties of compounds on their ADMET profiles. *Bioorganic & Medicinal Chemistry Letters*, *36*, 127825. https://doi.org/10.1016/j.bmcl.2021.127825

[30] Vellur, S., Pavadai, P., Babkiewicz, E., Ram Kumar Pandian, S., Maszczyk, P., & Kunjiappan, S. (2023). An in silico molecular modelling-based prediction of potential Keap1 inhibitors from Hemidesmus indicus (L.) R. Br. against oxidative-stress-induced diseases. *Molecules*, *28*(11), 4541. https://doi.org/10.3390/molecules28114541

[31] Manzoor, H., Khan, M. U., Shabbir, C. A., Rehman, R., Alhegaili, A. S., Ullah, M. I., . . . , & Alameen, A. A. M. (2025). Computational identification and evaluation of novel PD-L1 inhibitors for cancer immunotherapy. *Scientific Reports*, *15*(1), 33787. https://doi.org/10.1038/s41598-025-01232-7

[32] Fantacuzzi, M., Paciotti, R., & Agamennone, M. (2024). A comprehensive computational insight into the PD-L1 binding to PD-1 and small molecules. *Pharmaceuticals*, *17*(3), 316. https://doi.org/10.3390/ph17030316

How to Cite: Singh, V. K., Sahu, N., & Sinha, R. P. (2026). Beyond Sunscreen Multitarget Docking of Mycosporine-Like Amino Acids (MAAs) for Anti-aging, Neuroprotection, and Immunomodulation. *Medinformatics*. https://doi.org/10.47852/bonviewMEDIN62028733